Journal of Materials Chemistry A

PAPER

View Article Online
View Journal | View Issue

Cite this: J. Mater. Chem. A, 2014, 2, 14973

Multifunctional perovskite capping layers in hybrid solar cells†

Nan Li,[a] Haopeng Dong,[a] Hua Dong,[b] Jiaoli Li,[c] Wenzhe Li,[a] Guangda Niu,[a] Xudong Guo,[a] Zhaoxin Wu[b] and Liduo Wang*[a]

Received 10th June 2014
Accepted 13th July 2014

DOI: 10.1039/c4ta02921f

www.rsc.org/MaterialsA

In this study, the crucial role of perovskites capping layers in the $TiO_2/CH_3NH_3PbI_3$ hybrid solar cells is investigated. The capping layers are realized by controlling the concentration of PbI_2 solutions in the sequential deposition process. The morphologies of the active layers are studied by high-resolution scanning electron microscopy (HR-SEM). The amount of perovskites in capping layers increases with the concentration of PbI_2 solution, and the coverage of perovskite capping layers on TiO_2 films is better developed. Except for the correlation between photocurrents and coverages of perovskite proposed by Snaith, we revealed a more detailed relationship between the photovoltaic performances and perovskite capping layers. It is noteworthy that UV-vis absorption increased with perovskites in capping layers. Moreover, according to the diffuse reflection spectra, light scattering, which is beneficial for the conversion efficiency of photons to electrons by directly preventing most of the incident light from transmitting out, is also enhanced due to both the emergence of larger-size particles in the capping layers and the higher effective dielectric coefficient. All of the aforementioned aspects result in high photocurrents up to 20.6 mA cm^{-2}. Efficiency as high as 10.3% is ultimately achieved by a simple control of PbI_2 concentration in the sequential deposition process.

1 Introduction

Organic–inorganic perovskites have spurred scientists' great interests in hybrid solar cells, due to the direct and tunable band gap, high absorption coefficients in the large range of visible light, and high carrier mobilities.[1–7] Park fabricated perovskite-sensitized liquid solar cells using 2–3 nm-sized $CH_3NH_3PbI_3$ nanocrystals as the sensitizers, with a power-conversion efficiency up to 6.54%.[8] However, the rapid dissolution of $CH_3NH_3PbI_3$ in the I_3^-/I^- electrolyte induced the serious instability of solar cells, which decreased the overall performances intensely under continued irradiation.[8,9] Grätzel then reported all-solid-state mesoscopic solar cells with lead iodide perovskite as the sensitizer, in which spiro-OMeTAD was added as the hole transporter.[10] The improved stability of perovskite contributed to a higher conversion efficiency of 9.7%. Snaith *et al.* replaced the mesoporous TiO_2 film with insulating Al_2O_3 prepared at a lower temperature, introducing a new concept known as meso-superstructured solar cells (MSSC), which generated open-circuit photovoltages of more than 1.1 volts and a power conversion efficiency of 10.9%.[11] Moreover, using the sequential deposition process instead of the one-step method in the preparation of $CH_3NH_3PbI_3$, Grätzel took better control over perovskite morphology and achieved excellent photovoltaic performances, with rather high efficiency up to 15%.[12] In addition to the solution-processed devices, Snaith fabricated a simple planar heterojunction perovskite solar cell by vapour deposition, of which the power conversion efficiency reached more than 15%.[13] Furthermore, Y. Yang proposed an incorporative preparation method of $CH_3NH_3PbI_3$ called a vapor-assisted solution process, through which they obtained perovskite films with well-defined grain structures and grain sizes up to microscale and efficiency up to 12.1%.[14] Thus far, perovskite solar cells have developed from dye-sensitized liquid devices to all-solid-state devices with a great deal of research on preparation methods,[10,12–14] photoanodes[15–17] and hole-transport materials.[18–21]

In the various kinds of perovskite solar cells, the morphology of perovskite films plays an important role for photovoltaic performances. Snaith elucidated that in the solution process, a "wetting layer" could be formed on the internal surface of the mesoporous film uniformly with a sufficiently low concentration.[11] As the concentration increased, an extra perovskite film,

[a]Key Lab of Organic Optoelectronics and Molecular Engineering of Ministry of Education, Department of Chemistry, Tsinghua University, Beijing, P.R. China. E-mail: chldwang@mail.tsinghua.edu.cn

[b]Key Laboratory of Photonics Technology for Information, Department of Electronic Science and Technology, School of Electronic & Information Engineering, Xi'an Jiaotong University, Xi'an, 710049, P.R. China

[c]State Key Lab of Polymer Physics and Chemistry, Institute of Chemistry, Chinese Academy of Sciences, Beijing, 100190, P.R. China

† Electronic supplementary information (ESI) available: SEM images, *J–V* curves, photovoltaic parameters and the effective dielectric coefficient of TiO_2/perovskite films. See DOI: 10.1039/c4ta02921f

known as the "capping layer," emerged on top of the filled mesoporous Al_2O_3. They obtained various coverages of the $CH_3NH_3PbI_{3-x}Cl_x$ capping layer on Al_2O_3 by controlling the annealing temperatures and thicknesses of the films.[22] Results showed that the highest photocurrents were attainable only with the highest perovskite surface coverages. However, the details of perovskites in the capping layer had not been considered in depth.

In this study, we mainly focus on the critical $CH_3NH_3PbI_3$ capping layer on top of the mesoporous TiO_2 film in solution-processed $TiO_2/CH_3NH_3PbI_3$ hybrid solid solar cells. Compared with the devices fabricated by Snaith, mesoporous TiO_2 is used as the electron transport material (ETM) because the effective diffusion length of electrons in $CH_3NH_3PbI_3$ is shorter than that in $CH_3NH_3PbI_{3-x}Cl_x$.[23] With an increase in the concentration of PbI_2 solutions, higher photocurrents are obtained only with higher coverages of the perovskite capping layer on TiO_2 films, which is in accordance with the dependence of photocurrents on perovskite coverages demonstrated by Snaith.[22] Based on this result, we proceed with further work on the perovskite capping layers and the increasing photocurrents. As the PbI_2 concentration increases, more perovskite particles in the capping layer and enhanced light scattering are observed. More particles result in higher absorption, and light scattering is beneficial for stronger light harvesting by preventing most of the incident light from directly transmitting out. Both aspects contribute to the increasing photocurrents. Through simply varying the solution concentration, we achieve power conversion efficiency up to 10.3%. The important reasons for the growing photocurrents are elaborated in view of the larger amounts of perovskites in the capping layers and the enhanced light scattering, as well as the higher coverage of capping layers.

2 Experimental section

2.1 Materials synthesis

Methylammonium iodide (CH_3NH_3I) was synthesized by mixing 30 mL of methylamine (40% in methanol, TCI) and 32.3 mL of hydroiodic acid (57 wt% in water, Aldrich) in a 250 mL round-bottomed flask at 0 °C, followed by stirring the mixture for 2 h. The precipitate was recovered by putting the solution on a rotavap and carefully removing the solvents at 50 °C. The yellowish raw product of CH_3NH_3I was washed with diethyl ether by stirring the solution for 30 min, a step which was repeated three times, and the CH_3NH_3I was finally recrystallized from a mixed solvent of diethyl ether and ethanol. After filtration, the solid was collected and dried at 60 °C in a vacuum oven for 24 h.

2.2 Solar cell fabrication

FTO glasses were cleaned in ethanol and deionized water alternately using an ultrasonic bath. Titanium(IV) isopropoxide (Ti$[OCH(CH_3)_2]_4$, Aldrich, 99.999%, 1 mL) was mixed with 2-methoxyethanol ($CH_3OCH_2CH_2OH$, Alfa Aesar, 99%, 5 mL) and ethanolamine ($H_2NCH_2CH_2OH$, Alfa Aesar, 98+%, 0.5 mL) to prepare the precursor of compact TiO_2 layers. After magnetic stirring at 80 °C for 2 h, the precursor was coated on FTO glasses by spin-coating under 3000 rpm for 30 s in air. The substrate was subsequently treated at 80 °C for 10 min and 500 °C for 30 min. Afterward, mesoporous TiO_2 films were deposited on the substrate by spin-coating TiO_2 paste (18NR-T, Dysol) under 5000 rpm for 30 s, which was followed by heating at 500 °C for 1 h. Later, the sintered TiO_2 films were immersed in 0.02 M aqueous $TiCl_4$ (Aladdin, 99.99%) solution at 70 °C for 1 h, then taken out and heated at 500 °C for 1 h. PbI_2 (99.9985%, Alfa Aesar) was dissolved in anhydrous *N*,*N*-dimethylformamide (DMF, 99.9%, Aldrich) with a series of concentrations from 300 mg mL^{-1} to 500 mg mL^{-1}. Considering that at a high concentration of 500 mg mL^{-1} without any additives, the solution was no longer stable, and PbI_2 crystals began to form at the bottom of the sample bottles after placement at room temperature for 2 h, we set 500 mg mL^{-1} as the highest concentration. $CH_3NH_3PbI_3$ was synthesized with a sequential deposition method reported by Grätzel.[12] First, PbI_2 solutions were spin-coated on $TiCl_4$-treated mesoporous TiO_2 films at 5000 rpm for 60 s, followed by heating the films at 70 °C for 30 min in the glove box. The films were then immersed in a solution of CH_3NH_3I in 2-propanol (10 mg mL^{-1}) for 60 s and rinsed with 2-propanol. After being dried at room temperature, the films were treated at 70 °C for 30 min. The hole-transport material (HTM) was composed of 72.3 mg 2,29,7,79-tetrakis-(*N*,*N*-di-*p*-methoxyphenyl-amine)-9,99-spirobifluorene (spiro-MeOTAD), 17.5 μL bis(trifluoromethane)sulfonimide lithium salt (LiTFSI, 99.95%, Aldrich)/acetonitrile (520 mg mL^{-1}) and 37.5 μL 4-*tert*-butylpyridine (TBP, 96%, Aldrich) in a solvent of 1 mL chlorobenzene (99.9%, Alfa Aesar). The $CH_3NH_3PbI_3$-sensitized TiO_2 films were coated with HTM solution by spin-coating at 4000 rpm for 30 s. For the counter electrode, a 60 nm thick Au was deposited on the top of the HTM layer by thermal evaporation.

2.3 Characterization

The morphologies of perovskite layers were characterized by high-resolution scanning electron microscopy (HR-SEM) (Jeol, JSM-7401F). X-ray diffraction (XRD) patterns were obtained with smart lab instruments CuKα radiation ($\lambda = 1.54$ Å). The UV-vis absorption spectra and diffuse reflectance spectra of mesoporous TiO_2 (mp-TiO_2)/perovskite films were used to test the absorption and diffuse reflection of perovskite-sensitized TiO_2 film with a Hitachi model U-3010 UV-vis spectrophotometer. Photocurrent–voltage (*J*–*V*) curves, incident photon-to-electron conversion efficiency (IPCE), and intensity-modulated photocurrent spectroscopy (IMPS) were performed by a ZAHNER CIMPS electrochemical workstation, Germany.

3 Results and discussion

3.1 Morphologies and crystal structure of perovskites in capping layers

To intuitively observe the morphological changes of perovskite capping layers with increasing PbI_2 concentrations, we took surface SEM images of the perovskite films, as shown in Fig. 1. Obviously, uniform perovskite capping layers were formed on the TiO_2 films, and with the larger amount of perovskites, the

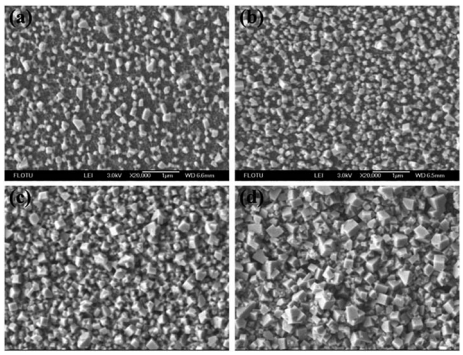

Fig. 1 SEM images of perovskite capping layers on mesoporous TiO_2 films with different concentrations of PbI_2 solutions: (a) 300 mg mL^{-1}, (b) 400 mg mL^{-1}, (c) 463 mg mL^{-1}, and (d) 500 mg mL^{-1}.

coverages of capping layers increased steadily from partially covered TiO_2 films to the complete coverage of perovskites with a PbI_2 concentration of 463 mg mL^{-1}. The larger amount of $CH_3NH_3PbI_3$ in capping layers is advantageous for higher light absorption, and the increasing coverage of perovskites can reduce recombination due to the decreasing possibilities of the direct contact between TiO_2 and spiro-OMeTAD.[13,14,22] However, as the concentration of PbI_2 solution was up to 500 mg mL^{-1}, more perovskite particles were aggregated and stacked, which was hard to control and easily to led to uneven morphologies and a small amount of voids, potentially increasing the recombination of electrons and holes. To further investigate the nature of perovskites formed on mesoporous TiO_2, X-ray diffraction (XRD) measurements were conducted with mp-TiO_2/perovskite films (Fig. 2). X-ray diffraction analysis for perovskites synthesized with different PbI_2 solutions showed diffraction peaks at 14.08°, 24.50°, 28.44° and 31.84°, which were assigned as the (100), (111), (200) and (210) lattice planes, respectively, of a cubic perovskite structure similar to the $CH_3NH_3PbI_3$ previously reported.[27] Moreover, peaks at 12.7° were ascribed to the formation of PbI_2. It is noteworthy that at higher PbI_2 concentrations, peak intensity became stronger, indicating the incomplete conversion to perovskites.

3.2 Enhanced light absorption and light scattering of perovskite capping layers

We tested UV-vis absorption spectra and diffuse reflection spectra of mp-TiO_2/perovskites films to study optical properties with different PbI_2 solutions. With higher concentrations of PbI_2 solutions, the enhanced absorption in the range of 450–750 nm were obtained, as illustrated in Fig. 3. Even at a low concentration of 300 mg mL^{-1}, a capping layer was formed on the TiO_2 film (Fig. 1(a)), indicating that the mesoporous film was probably filled up.[11] The larger amount of perovskites in the capping layer, as illustrated in the SEM images (Fig. 1), greatly improved the absorption. The drop of absorption at 500 nm was induced by the corrosion of $CH_3NH_3PbI_3$ in the air.[24] At lower concentrations, due to the smaller amount of perovskites and uncompleted coverage in the capping layer, more $CH_3NH_3PbI_3$ particles in mesoporous TiO_2 films were exposed to air, and the high specific surface area provided by mesoporous TiO_2 films accelerated the degradation of $CH_3NH_3PbI_3$. However, with complete coverage, the capping layer formed a barrier for the further contact between $CH_3NH_3PbI_3$ particles in mesoporous TiO_2 films and air, remarkably retarding the corrosion of $CH_3NH_3PbI_3$.

Moreover, from the SEM images, we found that as the concentration increased, larger perovskite particles appeared in the capping layer. More details can be seen in the cross-sectional SEM images illustrated in Fig. S1 (ESI†). The co-existence of big and small perovskite particles is beneficial to light scattering in the perovskite film, which contributes to a higher possibility for photons to be captured by preventing most of the incident light from transmitting out directly.[25,26] To confirm this, diffuse reflection spectra of perovskite-sensitized TiO_2 films were carried out, as shown in Fig. 4. Because perovskites had no absorption at the long wavelength range above 800 nm and TiO_2 photoanodes used in all devices were the same, differences between the reflectance data of perovskite on TiO_2 films clearly reflected the effects of light scattering in various

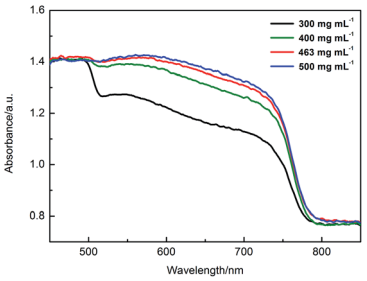

Fig. 3 UV-vis spectra of TiO_2/$CH_3NH_3PbI_3$ films.

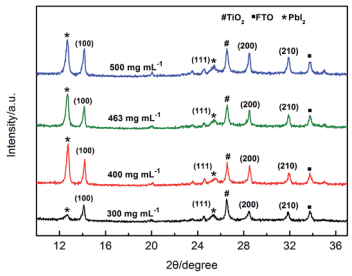

Fig. 2 X-ray diffraction (XRD) patterns of TiO_2/$CH_3NH_3PbI_3$ films.

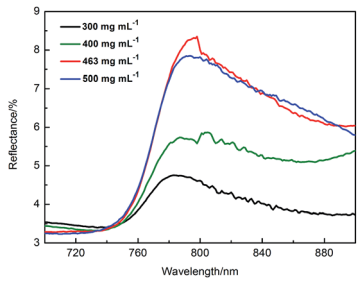

Fig. 4 Diffuse reflection spectra of TiO_2/$CH_3NH_3PbI_3$ films.

capping layers. Fig. 4 indicates that perovskite films prepared using 463 mg mL^{-1} and 500 mg mL^{-1} PbI_2 solutions show significantly improved scattering performances, consequently giving rise to the light harvesting. Moreover, the effective dielectric coefficient ε_m of mp-TiO_2/perovskites films can also affect light scattering. Table S1 (ESI†) shows an obvious change of the effective dielectric coefficient from 300 mg mL^{-1} to 400 mg mL^{-1}, whereas a slight increase was observed in the range of 400–500 mg mL^{-1}. According to Mie theory,[30] both the larger size of perovskite particles and the increased effective dielectric coefficient led to the enhancement of scattering (see details in ESI†). Because in the range of 400 mg mL^{-1} to 500 mg mL^{-1}, ε_m slightly changed but the size of perovskite particles obviously increased with PbI_2 concentration, we mainly contributed the enhanced reflectance at higher concentrations to the larger particle sizes in capping layers. Therefore, both the larger amount of perovskites in capping layers and the enhanced light scattering increased the light absorption, facilitating light harvesting and the possibility for incident photons converting into electrons.

3.3 Photovoltaic performances

Solar cells were fabricated by the aforementioned method in the Experimental section, with spiro-OMeTAD as the hole-transport material (HTM) and Au as the counter electrode. We have measured *J–V* characteristics of a batch of devices with the four concentrations under simulated air mass at 1.5 global (AM1.5G) solar irradiation, and the concentration of PbI_2 precursor solutions had remarkable impact on the photovoltaic performances, with details of the extracted performance parameters provided in Fig. S2 (ESI†). The results showed that as the concentration increased from 300 mg mL^{-1} to 463 mg mL^{-1}, the mean short circuit current J_{sc} rose from 15.2 mA cm^{-2} to 19.7 mA cm^{-2}, and the power conversion efficiency (PCE) rose from 6.9% to 9.2%. We mainly attributed the improved efficiency to the obviously increased J_{sc} because the fill factor (FF) and the open circuit voltage V_{oc} showed inconspicuous variations, compared with J_{sc}. Based on the former results, it is reasonable to attribute the improvement of photocurrents to the following aspects: stronger light harvesting with a larger amount of perovskites, higher coverage of capping layers, and improved light scattering facilitated by both the larger particle size in capping layers and the increased effective dielectric coefficient. Moreover, the mean parameter values, such as J_{sc} and the PCE of 500 mg mL^{-1} devices showed an obvious drop, ascribed to the increased recombination induced by the appearance of small voids observed in the Fig. 1(d), which was proved by the *J–V* curves in the dark condition (Fig. S3†).

However, the performance of the 500 mg mL^{-1} devices had a fluctuation above and below those of the 463 mg mL^{-1} devices in the same batch. Two reasons can explain this. First, the two concentrations were close, and the corresponding mp-TiO_2/perovskite films showed similar absorption (Fig. 3) and scattering (Fig. 4). Second, the solvent induced by the solution process probably influenced the growth and distribution of perovskite particles, particularly when excess perovskites aggregated in the capping layers at as high as a concentration of 500 mg mL^{-1}, and the change of capping layer morphologies affected devices performances. Therefore, for clear and accurate comparisons, we gave 300 mg mL^{-1} and 463 mg mL^{-1} as examples to show the effects of capping layers on photovoltaic performances. The best performing *J–V* curves are depicted in Fig. 5. As the concentration increased from 300 mg mL^{-1} to 463 mg mL^{-1}, the short circuit current J_{sc} reached as high a value as 20.6 mA cm^{-2}, and the power conversion efficiency (PCE) rose from 7.9% to 10.3% by 30.4%.

To fully study the increase of photocurrents, we discussed the electron transfer in devices by measuring IMPS spectra with the electrochemical workstation. IMPS spectra measure the photocurrent response of the device to a small sinusoidal perturbation of the light intensity superimposed on a larger steady background level, providing information about the dynamics of charge transport.[28] As is shown in Fig. 6(a), the electron diffusion coefficient increased as the concentration rose from 300 mg mL^{-1} to 463 mg mL^{-1}, indicating that the electron transfer was accelerated. The incident photon-to-current efficiency (IPCE) spectra were also carried out to investigate the ratio of extracted electrons to incident photons at a given wavelength. Fig. 6(b) shows that in the range from 400 nm

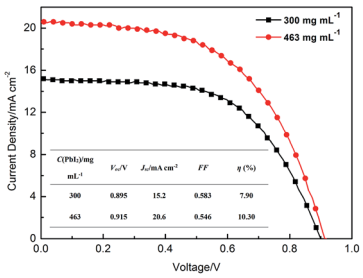

Fig. 5 *J–V* curves of the 300 mg mL^{-1} and the 463 mg mL^{-1} devices in the best performing batch under simulated AM1.5G solar irradiation.

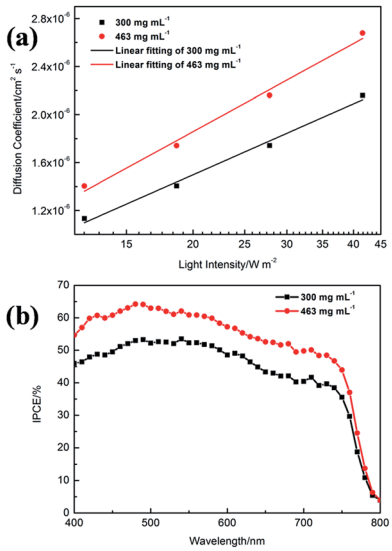

Fig. 6 (a) IMPS spectra and (b) IPCE spectra of photovoltaic devices.

to 750 nm, IPCE increased with the rise of concentrations from 300 mg mL^{-1} to 463 mg mL^{-1}. As we know, IPCE is determined by the following equation,[29] expressed as

$$IPCE(\lambda) = LHE(\lambda)\varphi_{inj}\eta_{coll},$$

where LHE (λ) is the light-harvesting efficiency for photons of wavelength λ, φ_{inj} is the quantum yield for the electron injection from the light harvester to the conduction band of the semiconductor oxide, and η_{coll} is the electron collection efficiency.

A higher concentration of PbI_2 solutions leads to higher LHE due to the larger amount of perovskites and stronger light scattering, verified by UV-vis spectra and diffuse reflection spectra. The accelerated electron derived from IMPS is favorable to the rise of φ_{inj} and η_{coll}. However, because the effective diffusion length of triiodide perovskite is on the order of 100 nm,[6] capping layers with excess thickness may interfere with the electron injection into TiO_2 films, thus decreasing φ_{inj} and η_{coll}. Optimizing the thickness of the perovskite capping layer may achieve both efficient electron transfer and strong light harvesting. Nevertheless, the enhanced IPCE values prove that LHE has sufficient increase by which to compensate for the loss of φ_{inj} and η_{coll}. This gives reasonable explanations for the increasing photocurrents.

4 Conclusions

By controlling the concentration of PbI_2 solutions in the sequential deposition process, we have fabricated a series of hybrid perovskite solar cells. In this work, we mainly focused on the capping layers of perovskite films, which attracted little attention in previous studies. The effects of capping layers on perovskite morphologies and photovoltaic performances of devices were carefully investigated. It has been demonstrated that the capping layer plays a critical role in perovskite solar cells with light absorption and scattering of $CH_3NH_3PbI_3$ particles. As the concentration of PbI_2 solutions rises, we obtain a higher coverage of perovskite capping layers on the mesoporous TiO_2 films, which can decrease the charge recombination, and a larger amount of perovskites in the capping layer and enhanced light scattering, both of which improve the light absorption. All aspects previously presented are beneficial for the photocurrents, resulting in the highest values, up to 20.6 mA cm^{-2}. By optimizing the concentration of PbI_2 solutions and perovskite capping layers, the efficiency of 10.3% has been achieved. The impacts of the perovskite capping layer on the performances of hybrid perovskite solar cells are astounding. By optimizing the thickness of perovskite capping layers, we expect that a higher efficiency can be achieved, and this part of the research is proceeding in our lab.

Acknowledgements

This work was supported by the National Natural Science Foundation of China under Grant no. 51273104 and the National Key Basic Research and Development Program of China under Grant no. 2009CB930602.

Notes and references

1 J. H. Heo, S. H. Im, J. H. Noh, T. N. Mandal, C.-S. Lim, J. A. Chang, Y. H. Lee, H.-j. Kim, A. Sarkar, M. K. Nazeeruddin, M. Grätzel and S. I. Seok, *Nat. Photonics*, 2013, **7**, 486–491.
2 J. H. Noh, S. H. Im, J. H. Heo, T. N. Mandal and S. I. Seok, *Nano Lett.*, 2013, **13**, 1764–1769.
3 N. G. Park, *J. Phys. Chem. Lett.*, 2013, **4**, 2423–2429.
4 G. Xing, N. Mathews, S. Sun, S. S. Lim, Y. M. Lam, M. Gratzel, S. Mhaisalkar and T. C. Sum, *Science*, 2013, **342**, 344–347.
5 H. J. Snaith, *J. Phys. Chem. Lett.*, 2013, **4**, 3623–3630.
6 S. D. Stranks, G. E. Eperon, G. Grancini, C. Menelaou, M. J. Alcocer, T. Leijtens, L. M. Herz, A. Petrozza and H. J. Snaith, *Science*, 2013, **342**, 341–344.
7 M. He, D. Zheng, M. Wang, C. Lin and Z. Lin, *J. Mater. Chem. A*, 2014, **2**, 5994–6003.
8 J. H. Im, C. R. Lee, J. W. Lee, S. W. Park and N. G. Park, *Nanoscale*, 2011, **3**, 4088–4093.
9 L. Etgar, P. Gao, Z. Xue, Q. Peng, A. K. Chandiran, B. Liu, M. K. Nazeeruddin and M. Grätzel, *J. Am. Chem. Soc.*, 2012, **134**, 17396–17399.
10 H. S. Kim, C. R. Lee, J. H. Im, K. B. Lee, T. Moehl, A. Marchioro, S. J. Moon, R. Humphry-Baker, J. H. Yum, J. E. Moser, M. Grätzel and N. G. Park, *Sci. Rep.*, 2012, **2**, 591.
11 M. M. Lee, J. Teuscher, T. Miyasaka, T. N. Murakami and H. J. Snaith, *Science*, 2012, **338**, 643–647.
12 J. Burschka, N. Pellet, S. J. Moon, R. Humphry-Baker, P. Gao, M. K. Nazeeruddin and M. Grätzel, *Nature*, 2013, **499**, 316–319.
13 M. Liu, M. B. Johnston and H. J. Snaith, *Nature*, 2013, **501**, 395–398.
14 Q. Chen, H. Zhou, Z. Hong, S. Luo, H. S. Duan, H. H. Wang, Y. Liu, G. Li and Y. Yang, *J. Am. Chem. Soc.*, 2014, **136**, 622–625.
15 S. Dharani, H. K. Mulmudi, N. Yantara, P. T. Thu Trang, N. G. Park, M. Grätzel, S. Mhaisalkar, N. Mathews and P. P. Boix, *Nanoscale*, 2014, **6**, 1675–1679.
16 H. S. Kim, J. W. Lee, N. Yantara, P. P. Boix, S. A. Kulkarni, S. Mhaisalkar, M. Grätzel and N. G. Park, *Nano Lett.*, 2013, **13**, 2412–2417.
17 P. Qin, A. L. Domanski, A. K. Chandiran, R. Berger, H. J. Butt, M. I. Dar, T. Moehl, N. Tetreault, P. Gao, S. Ahmad, M. K. Nazeeruddin and M. Grätzel, *Nanoscale*, 2014, **6**, 1508–1514.
18 A. Abate, D. J. Hollman, J. Teuscher, S. Pathak, R. Avolio, G. D'Errico, G. Vitiello, S. Fantacci and H. J. Snaith, *J. Am. Chem. Soc.*, 2013, **135**, 13538–13548.
19 A. Abrusci, R. S. Santosh Kumar, M. Al-Hashimi, M. Heeney, A. Petrozza and H. J. Snaith, *Adv. Funct. Mater.*, 2011, **21**, 2571–2579.
20 D. Bi, L. Yang, G. Boschloo, A. Hagfeldt and E. M. J. Johansson, *J. Phys. Chem. Lett.*, 2013, **4**, 1532–1536.
21 J. A. Christians, R. C. Fung and P. V. Kamat, *J. Am. Chem. Soc.*, 2014, **136**, 758–764.

22 G. E. Eperon, V. M. Burlakov, P. Docampo, A. Goriely and H. J. Snaith, *Adv. Funct. Mater.*, 2014, **24**, 151–157.
23 E. Edri, S. Kirmayer, A. Henning, S. Mukhopadhyay, K. Gartsman, Y. Rosenwaks, G. Hodes and D. Cahen, *Nano Lett.*, 2014, **14**, 1000–1004.
24 G. Niu, W. Li, F. Meng, L. Wang, H. Dong and Y. Qiu, *J. Mater. Chem. A*, 2014, **2**, 705.
25 Y. Shi, C. Zhu, L. Wang, W. Li, C. Cheng, K. M. Ho, K. K. Fung and N. Wang, *J. Mater. Chem.*, 2012, **22**, 13097.
26 C. Zhu, Y. Shi, C. Cheng, L. Wang, K. K. Fung and N. Wang, *J. Nanomater.*, 2012, **2012**, 1–8.
27 T. Baikie, Y. Fang, J. M. Kadro, M. Schreyer, F. Wei, S. G. Mhaisalkar, M. Grätzel and T. J. White, *J. Mater. Chem. A*, 2013, **1**, 5628.
28 J. Krüger, R. Plass, M. Grätzel, P. J. Cameron and L. M. Peter, *J. Phys. Chem. B*, 2003, **107**, 7536–7539.
29 M. Grätzel, *Acc. Chem. Res.*, 2009, **42**, 1788–1798.
30 J. R. Lakowicz, *Anal. Biochem.*, 2005, **337**, 171–194.